A Numerical Study of Stratified Tidal Rectification over Finite-Amplitude Banks. Part II: Georges Bank*

CHANGSHENG CHEN,† ROBERT C. BEARDSLEY, AND RICHARD LIMEBURNER

Department of Physical Oceanography, Woods Hole Oceanographic Institution, Woods Hole, Massachusetts

(Manuscript received 15 April 1993, in final form 6 January 1995)

ABSTRACT

Tidal rectification over an idealized two-dimensional cross section of Georges Bank, which is a large, shallow, elongated submarine bank in the Gulf of Maine, is studied using a primitive equation coastal ocean circulation model. In the homogeneous case, the model predicts a topographically controlled residual circulation over Georges Bank, flowing northeastward as a strong jet with a maximum speed of about 16 cm s^{-1} along the northern flank and southwestward as a relatively weak and broad flow with a maximum speed of about 3 cm s^{-1} on the southern flank. As stratification is added, tidal rectification and tidal mixing intensify the along- and cross-isobath residual currents and create tidal fronts. During summer, the tidal fronts are located at the 40-m isobath on the northern flank and at the 50–60-m isobath on the southern flank, while during winter, the position of the tidal front remains fixed on the northern flank; however, it moves to the shelf break on the southern flank. The summer and winter maxima of the along-bank current are about 32 cm s^{-1} and 26 cm s^{-1} on the northern flank and 8 cm s^{-1} and 6 cm s^{-1} on the southern flank, respectively. The model results are in reasonable agreement with observations. The summertime intensification of the residual flow is mainly due to nonlinear interaction between the stratified tidal currents over the northern flank with the steep bottom topography there and to the baroclinic density gradient created in part by tidal mixing over the southern flank where the bottom slope is smaller.

1. Introduction

Long-term direct Eulerian and Lagrangian current measurements summarized by Butman et al. (1987) clearly demonstrate a clockwise circulation around Georges Bank, which varies seasonally with a maximum in the along-bank flow in summer and fall and a minimum in winter (upper panel in Fig. 1). Trajectories of satellite-tracked surface drifters drogued at 5 m obtained by Limeburner and Beardsley (1989) nicely illustrate the partially closed nature of the along-bank circulation in summer (hence the term "gyre") caused by recirculation of water, flowing southwestward along the southern flank and turning northward through the Great South Channel to feed the narrow northeastward jet on the northern flank (lower panel in Fig. 1). Seasonal intensification of the along-bank mean circulation is associated with the seasonal variation in stratification over the bank. The clockwise circulation around the bank appears most pronounced at the surface in late summer and fall when the vertical density stratification is strongest over the flanks of the bank. Hydrographic observations show tidal mixing fronts between the vertically well-mixed and stratified waters over Georges Bank and a shelf/slope front between the relatively fresh shelf water and the more saline upper slope water along the southern edge of the bank (Fig. 2). During late spring and summer, the fronts are located along the 40-m isobath on the northern flank and along the 50–60-m isobath on the southern flank (Fig. 2b). During winter, however, the tidal front disappears on the southern flank and is much weaker on the northern flank, even though the position of this front remains almost stationary on the northern edge of the bank (Fig. 2a). The shelf/slope front occurs at the shelf break near the 100-m isobath on the southern flank and appears to move steadily onshore from winter to summer and then suddenly readjusts offshore as fall turns to winter (Flagg 1987). As a result, the along-bank residual flow intensifies during summer and fall on the northern edge of the bank, over the top of the bank, and near the shelf break on the southern flank where the stronger tidal and shelf/slope fronts are located.

A numerical study of stratified tidal rectification over a finite-amplitude, two-dimensional symmetric bank was recently conducted by Chen and Beardsley (1994) using a modified version of the Blumberg and Mellor

* Woods Hole Oceanographic Institution Contribution No. 8215.

† Current affiliation: Department of Marine Sciences, University of Georgia, Athens, Georgia.

Corresponding author address: Dr. Robert C. Beardsley, Department of Physical Oceanography, Woods Hole Oceanographic Institution, Woods Hole, MA 02543.

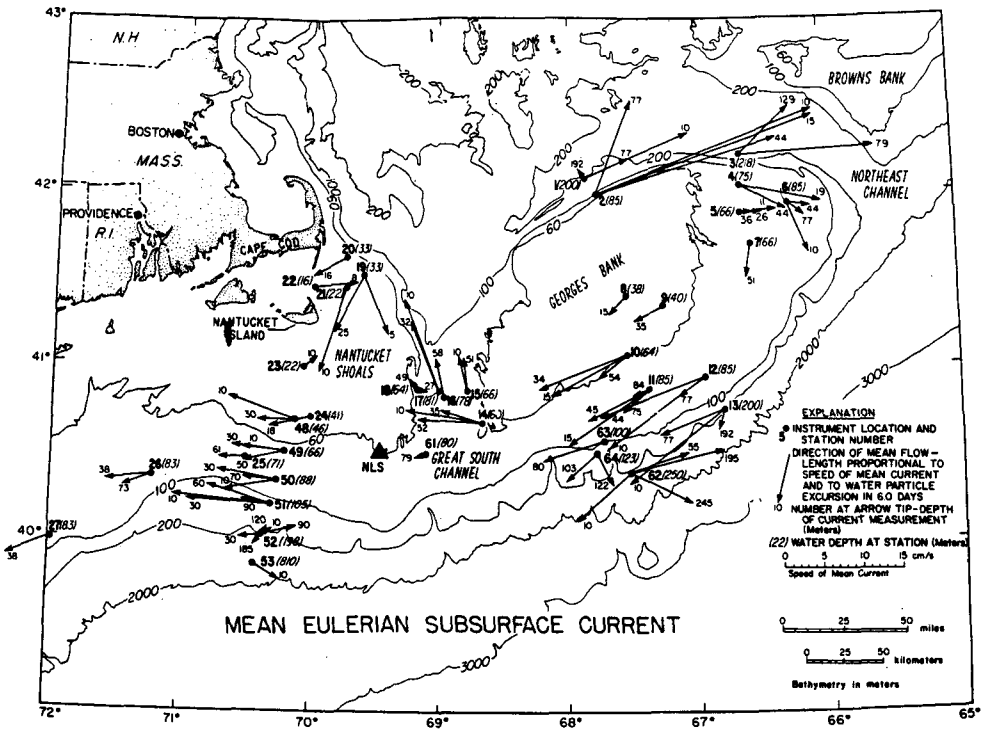

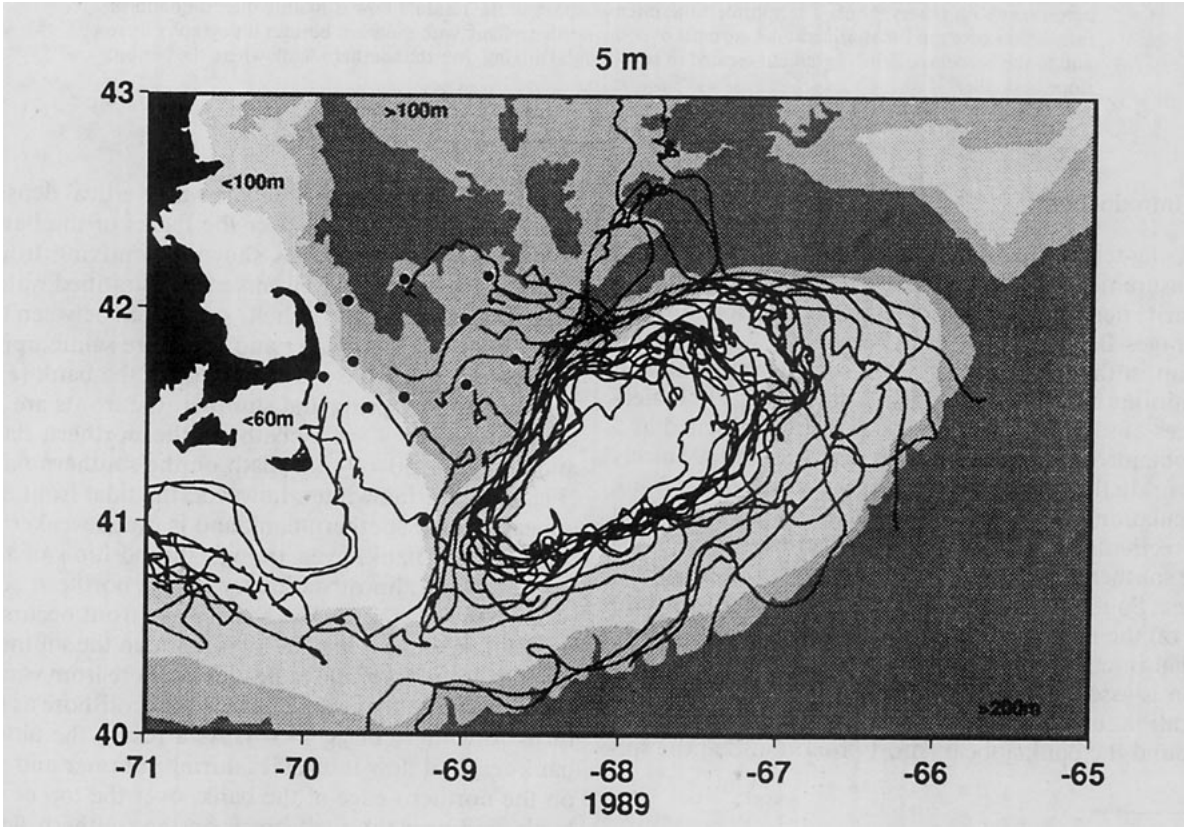

FIG. 1. Mean Eulerian current measurements made during 1975–1981 summarized by Butman et al. (1982) (upper panel), and trajectories of satellite-tracked surface drifters drogued at 5 m deployed by Limeburner and Beardsley in June 1989 in the western Gulf of Maine (lower panel). In the upper panel, the boldface numbers at origins of the current vectors are station identifiers, italic numbers in parentheses indicate water depth (m), numbers at the tips of arrows indicate depth of measurement (m), and the speed scale is such that the length of current vector is equivalent to the mean displacement of a water particle during a 6-day period at map scale. In the lower panel, the solid dots represent the initial deployment positions concentrated in the northern Great South Channel region, and the solid lines the low-pass filtered drifter trajectories. Note that many of the drifters make several circuits around the top of Georges Bank before flowing south off the bank or westward into the Mid-Atlantic Bight. The topography is shaded to indicate depth ranges, with transitions demarking the 60-m, 100-m, and 200-m isobaths.

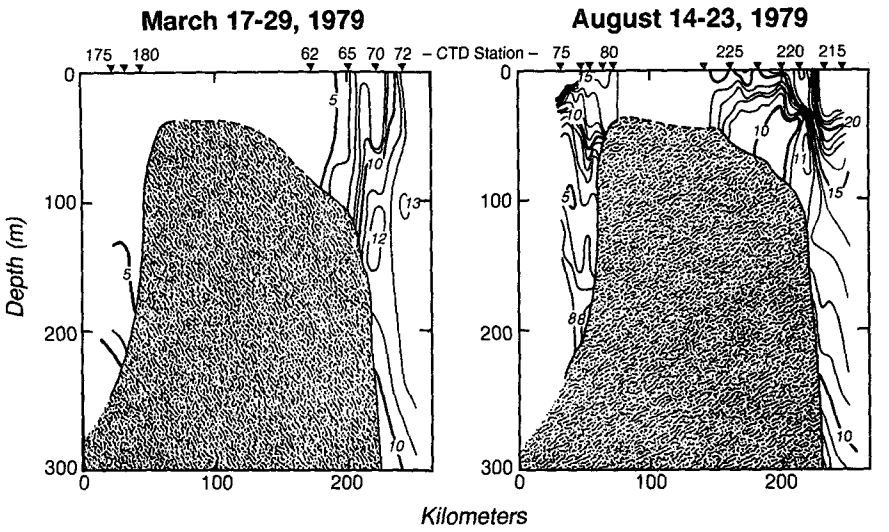

FIG. 2. Cross-bank transects of temperature (°C) during (a) 17–29 March 1979 and (b) 14–23 August 1979. Combined CTD and XBT data were used in these plots (redrawn from Flagg 1987).

(1987) coastal ocean circulation model. Initial value experiments were conducted in which a barotropic M_2 tide was generated at the ocean boundary of the model and allowed to propagate across the bank. After an initial adjustment period of several tidal periods, the model reaches a quasi-steady state consisting of the tidal and residual flow fields. Numerical experiments with both homogeneous and linear initial stratification clearly demonstrate the importance of three processes that contribute to driving residual flow in stratified tidal rectification: 1) the formation of a tidal front due to turbulent mixing, 2) the generation of internal waves at tidal and higher frequencies over the slope, and 3) the modification of internal friction by stratification. In particular, the experiments indicate that the horizontal density gradient at the tidal front and nonlinear interaction between stratified tidal currents both contribute significantly to the summertime intensification of the residual flow over a finite-amplitude symmetric bank.

The actual bottom topography of Georges Bank is quite asymmetric, however, with the northern flank being quite steep in comparison with the southern flank. In this paper, we use the numerical model approach developed in Part I to investigate the effects of an asymmetric bottom topography on the resultant stratified tidal rectification over an idealized cross section of Georges Bank. Since the experimental conditions (e.g., tidal forcing, approximate height and width of bank, and initial stratification) used in Part I were chosen to crudely model Georges Bank, we expect the three basic processes found in Part I that influence stratified tidal rectification to occur in this study with more realistic bottom topography. While we will find this to be true, the locations of the tidal fronts and relative importance of the different driving mechanisms are dependent on the shape of the bottom, and thus influence the structure of the residual flow over Georges Bank. While the observed subtidal flow on Georges Bank is fully three-dimensional (as shown in Fig. 1), Loder (1980) has shown that detailed study of two-dimensional dynamics can provide good insight into physical processes over the northern and southern flanks of the bank. This model study has a similar objective, that is, to examine the influence of realistic cross-bank bottom topography on stratified tidal rectification and mixing in a simplified two-dimensional case without the added complexity of fully three-dimensional bank topography.

This paper consists of six sections. The design of the numerical experiment is described in section 2. The model results for homogeneous, winter and summer stratification cases are given in section 3, followed by comparison between the model-predicted and observed residual currents on Georges Bank in section 4. A diagnostic analysis of momentum and heat balances is made in section 5 to examine the different driving mechanisms of stratified tidal rectified flow over an asymmetric bank. Finally, conclusions are given in section 6.

2. Design of numerical experiments

The numerical model used in this study is a modified version of the three-dimensional coastal ocean circulation model developed by Blumberg and Mellor (1987). This model incorporates the Mellor and Yamada (1982) level 2 1/2 turbulent closure model to provide a realistic parameterization of vertical mixing and a free surface to simulate long surface gravity waves. The model uses a σ-coordinate system in the vertical and a nonuniform coordinate system in the horizontal.

Unlike the original Blumberg and Mellor (1987) time-splitting code, the version used here incorporates a semi-implicit scheme in the horizontal for the barotropic mode developed by Casulli (1990). This semi-implicit method improves the computational efficiency with a single time step for both barotropic and baroclinic motion. This semi-implicit version (called ECOM-si) is described in detail by Blumberg (1992), and the two-dimensional version used in this study is described in Part I.

The model domain features a cross-bank section cut from southeast to northwest across the center of Georges Bank (Fig. 3). The bottom topography along the section is taken from Uchupi and Austin (1987). The numerical model grid is shown in Fig. 4 where a nonuniform grid is used in the horizontal and an uniform grid in the vertical. The horizontal resolution is 1.0 km near and on the bank and linearly increases to 11.96 km over an interval of 15 grid points outside the domain of interest. The vertical resolution in the σ-coordinate system is $\Delta\sigma = 0.033$ (31 points in the vertical), which corresponds to a vertical Δz of 10 m in the deep offbank region with a constant depth of H_d = 300 m and 4–1.3 m over the bank with a depth of H_s, varying from 120 to 40 m.

The model is forced by the barotropic M_2 tidal elevation at the southern open boundary. Also, a gravity wave radiation boundary condition with a propagation speed of $\sqrt{gH_d}$ (plus a sponge layer) is specified at the northern open boundary to allow the tidal wave to propagate out of the computational domain with minimum reflection [see Chapman (1985) for a detailed discussion]. Initial experiments with a homogeneous fluid show a relatively strong surface wave reflection on the southern side of the bank, which reduced by about half the amplitude of the incident tidal current in the deep region and thus reduced the tidal mass transport across the bank. Occurrence of the reflected wave is believed to be due to the very steep bottom topography on either side of the bank, a process which can be interpreted using a simple theory of long gravity wave reflection over step topography (LeBlond and Mysak 1978). Since our focus is on simulating flow conditions over the bank, we have adjusted the surface forcing at the southern open boundary so that the combined incident and reflected tidal waves produce the desired tidal mass transport across the bank. In this geometry, a forcing amplitude of $\zeta_0 = 90$ cm produces a cross-bank barotropic surface tidal current of about 12 cm s^{-1} in the deep region and about 90 cm s^{-1} over the top of the bank, consistent with tidal current measurements over Georges Bank reported by Moody et al. (1984).

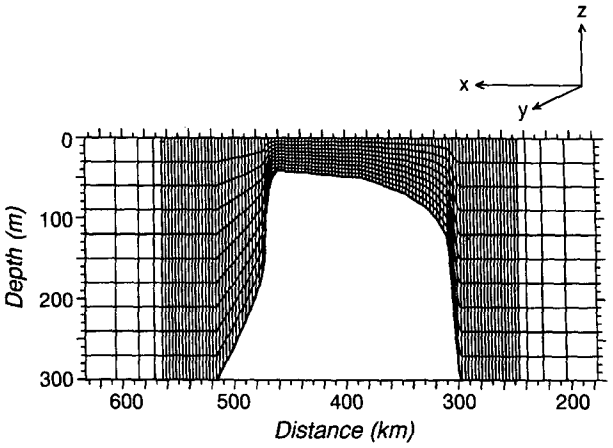

FIG. 4. Numerical grid for Georges Bank model plotted every three points in both the horizontal and the vertical. The horizontal and spacing is 1.0 km near and across the bank from 249 to 561 km and then linearly increases to 11.96 km over an interval of 15 grid points outside of the domain of interest. The vertical grid spacing for σ is $\Delta\sigma = 0.033$. The shallowest water depth is 40 m at 460 km away from the southeastern open boundary.

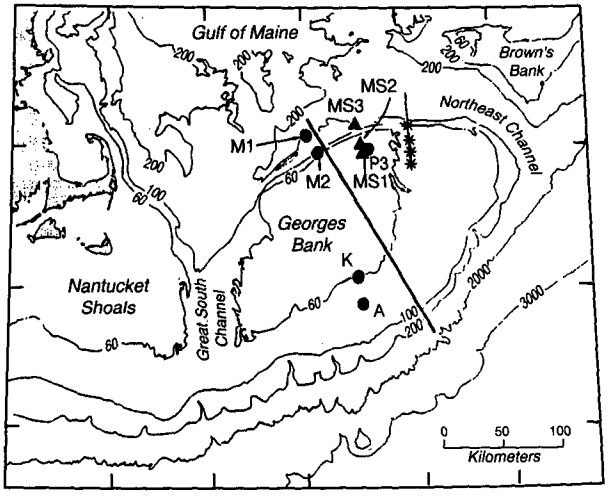

FIG. 3. Bathymetry (in meters) of the southern New England continental margin (Uchupi and Austin 1987). The heavy solid line is the section for our numerical experiment, and light solid line (marked L) is the 1988 CTD, ADCP, and moored current meter measurement section conducted by Loder et al. (1992). Solid circles with capital letters and numbers are moored current meter stations identified in Butman et al. (1982). Solid triangles and asterisks are moored current meter stations deployed by Marsden (1986) and Loder et al. (1992), respectively.

The model has been run as an initial value problem with homogeneous, winter (weak) and summer (strong) stratification. The initial temperature distribution for summer and winter stratification is simply given by a linear function of z based on data from the summer and winter 1979 hydrographic sections reported by Flagg (1987). The initial surface and bottom (at depth of 300 m) temperatures are taken as 20° and 11°C for the summer case and 13° and 11°C for the winter case. To simplify the model problem and focus on the effects of tidal mixing in producing thermal fronts, we ignore the spatial structure of the background salinity and make salinity constant (35‰) throughout

the computational domain. The resulting initial Brunt–Väisälä frequency N is equal to 3×10^{-3} s^{-1} and 10^{-2} s^{-1} for winter and summer stratification cases, respectively. To avoid transients due to sharp initial conditions, we ramp up the model tidal forcing from zero to full value over 1 1/2 days. Once the tidal currents and density fields reach a quasi-equilibrium state, the residual flow and mean temperature fields are obtained by averaging over one tidal cycle.

3. Model results

a. *Structure of along-bank residual current*

Figure 5 shows the structure of along-bank residual current and mean temperature in the homogeneous, winter and summer stratification cases across Georges Bank. In the homogeneous case, the model predicts a topographically controlled residual current over the bank, flowing northeastward as a strong jet with a maximum speed of about 16 cm s^{-1} along the northern flank and southwestward as a relatively weak and broader flow with a maximum of about 3 cm s^{-1} at the 50-m isobath from the top of the bank to the southern flank (Fig. 5a). As weak stratification is included during winter, the strong tidal currents vertically mix the water column over the top of the bank, creating a tidal-mixing front near the shelf break at about the 70-m isobath on the northern flank and at the 90-m isobath on the southern flank (Fig. 5b). Correspondingly, the winter along-bank residual current intensifies at the fronts near the shelf break on both sides of the bank, with a maximum of about 6 cm s^{-1} on the southern flank and of about 26 cm s^{-1} on the northern flank (Fig. 5c). Similar to the homogeneous case, the alongbank current is still intensified at the surface. However, there are two maximum southwestward velocities on the southern flank: one associated with the topography-induced barotropic tidal rectification over the bank (as seen in Fig. 5a) and the other due to the tidal mixing front during winter.

Increased stratification in summer inhibits tidal mixing over the bank, so that the location of the tidal mixing front shifts to the 40-m isobath at the shelf break on the northern flank and to the 60-m isobath on the southern flank (Fig. 5d). The tidally mixed bottom boundary layer is clearly identified over the southern flank south of the tidal mixing front. The thickness of this bottom boundary layer decreases seaward as the water depth increases and finally disappears near the shelf break. Correspondingly, the along-bank residual current intensifies along the axis of maximum baroclinic temperature gradient (the top of the bottom mixed layer) on the southern flank and near the shelf break on the northern flank (Fig. 5e). The maximum along-bank residual current increases to 32 cm s^{-1} at a depth of about 20 m, about 7 km to the north of the shelf break on the northern flank, and to 8 cm s^{-1} at a height of 27 m above the bottom, about 10 km inside of the shelf break on the southern flank. In contrast to the upper mean circulation pattern, the along-bank residual current below 200 m near the bottom is weak and flows in a counterclockwise sense along the bank with recirculation farther offbank, thus forming weak anticyclonic-like eddies in the deep water both north and south of the bank. Since no strong vertical mixing is found beyond the slope, the existence of the deep eddylike mean circulation is due in part to internal wave reflection as discussed in Chen (1992).

b. *Structure of cross-bank residual current*

Figures 6 and 7 show the distribution of the residual cross-bank velocity ($\bar{u}$) and vertical velocity ($\bar{w}$) on the southern and northern flanks of Georges Bank for homogeneous, winter and summer stratification cases, respectively. In the homogeneous case, the predicted cross-bank residual current is characterized by a single circulation cell on either side of the bank where the water tends to be upwelled along the sloping bottom and then downwelled over the outer flank. The maximum upwelling velocity is about 2.8×10^{-2} cm s^{-1} on the northern flank and 4×10^{-3} cm s^{-1} on the southern flank, while the maximum downwelling velocity is about 2.2×10^{-2} cm s^{-1} on the northern side of the shelf break on the northern flank and 3×10^{-3} cm s^{-1} on the southern side of the shelf break (Figs. 6b and 7b) on the southern flank. The water over the top of the bank tends to flow southward off the bank at all depths with a maximum velocity of 0.6 cm s^{-1} at the surface near the northern flank and decreasing as the water becomes deeper (Figs. 6a and 7a).

Unlike the homogeneous case, the wintertime cross-bank residual current is mainly dominated by a double circulation cell pattern centered at the tidal mixing front on both sides of the bank (Figs. 6c,d and 7c,d). The maximum of cross-bank and vertical residual currents is about 1.8 cm s^{-1} in $\bar{u}$ and either -0.08 cm s^{-1} in $\bar{w}$ at a depth of 60 m in the downwelling region or 0.05 cm s^{-1} in $\bar{w}$ at a depth of 56 m in the upwelling region on the southern flank, while it is about 3.5 cm s^{-1} in $\bar{u}$ and either -0.12 cm s^{-1} in $\bar{w}$ at a depth of 70 m in the downwelling region along the slope or 0.18 cm s^{-1} in $\bar{w}$ at a depth of 83 m in the upwelling region on the northern flank.

The summertime cross-bank circulation exhibits a strong asymmetry with respect to the two sides of the bank. On the southern side, the cross-bank current is characterized by multiple circulation cells, which are strongest near the shelf break where the bottom slope becomes steep and mixing is weak and become weaker as the water becomes shallower and vertical mixing increases (Figs. 6e, f). The magni-

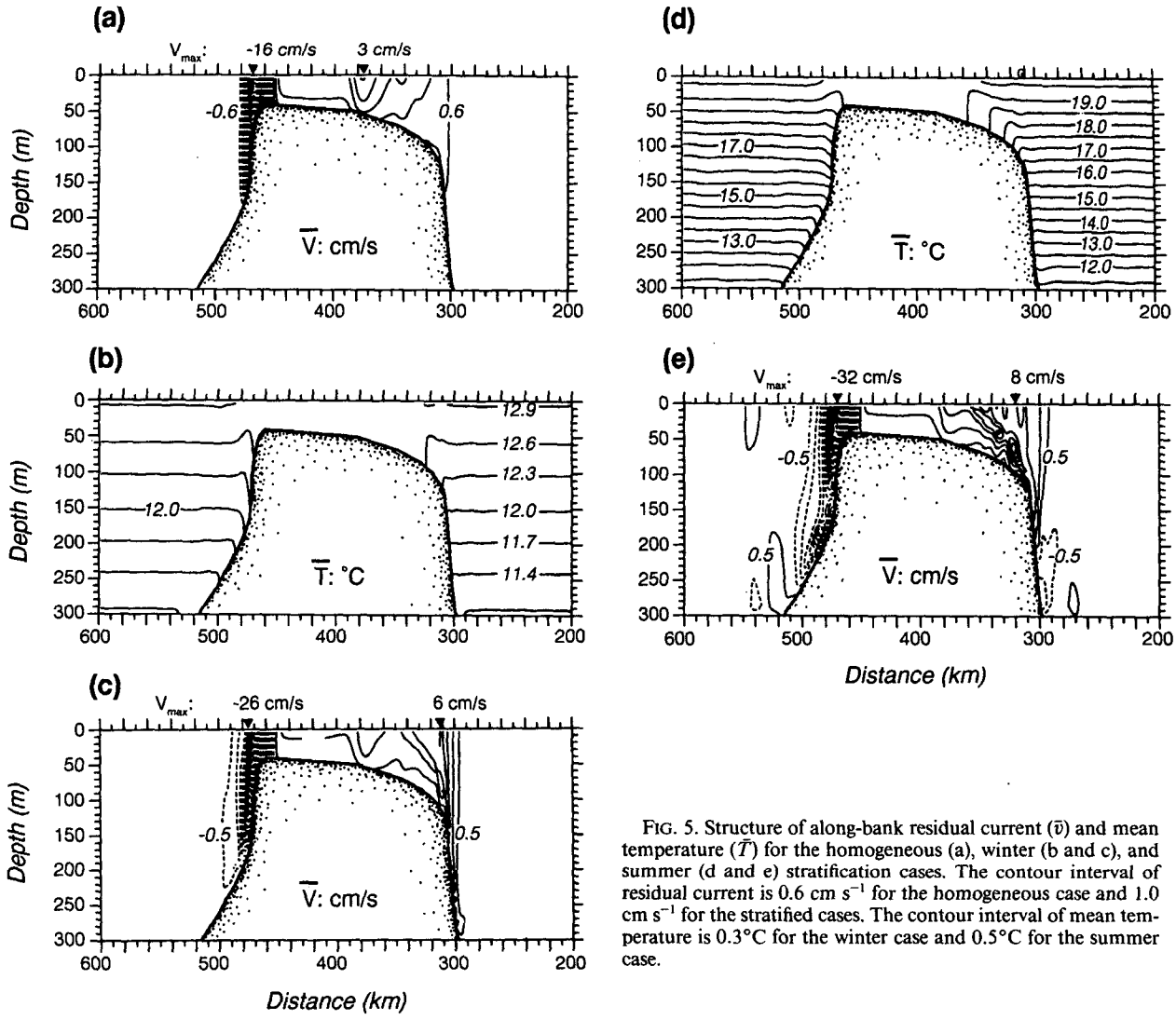

FIG. 5. Structure of along-bank residual current ($\bar{v}$) and mean temperature ($\bar{T}$) for the homogeneous (a), winter (b and c), and summer (d and e) stratification cases. The contour interval of residual current is 0.6 cm s^{-1} for the homogeneous case and 1.0 cm s^{-1} for the stratified cases. The contour interval of mean temperature is 0.3°C for the winter case and 0.5°C for the summer case.

tudes of the cross-bank and vertical residual currents are about 5 cm s^{-1} in $\bar{u}$ and 0.1 cm s^{-1} in $\bar{w}$ at a depth of 120 m near the shelf break and decrease to 0.5 cm s^{-1} in $\bar{u}$ and 0.01 cm s^{-1} in $\bar{w}$ at the tide-induced thermal front. On the northern side, however, the cross-bank current is dominated by a single strong circulation cell centered at the tidal front where the water is carried down along the sloping bottom to about 150 m deep and then upwelled again to the northern side of the front (Figs. 7e, f). The maximum velocity is about 10 cm s^{-1} in $\bar{u}$ and −0.3 cm s^{-1} in $\bar{w}$, occurring at a depth of 50 m near the shelf break and near the surface on the northern side of the front. Over the top of the bank inside the fronts where water is vertically well mixed, the residual current is quite similar to that in the homogeneous case, flowing southward off the bank at all depths at a speed of about 0.6 cm s^{-1} at the surface and 0.1 cm s^{-1} near the bottom.

c. *Distribution of mean surface elevation and vertical eddy viscosity*

Figure 8 shows the cross-bank distribution of mean surface elevation for homogeneous, winter, and summer stratification cases. For all cases, the mean surface elevation tends to increase northward over the top of bank and then fall sharply at the edge of the northern flank. The gradient of mean surface elevation on the top of bank is 0.7×10^{-8} in the homogeneous case but increases up to 0.3×10^{-7} in winter and 0.7×10^{-7} in summer. This positive sur-

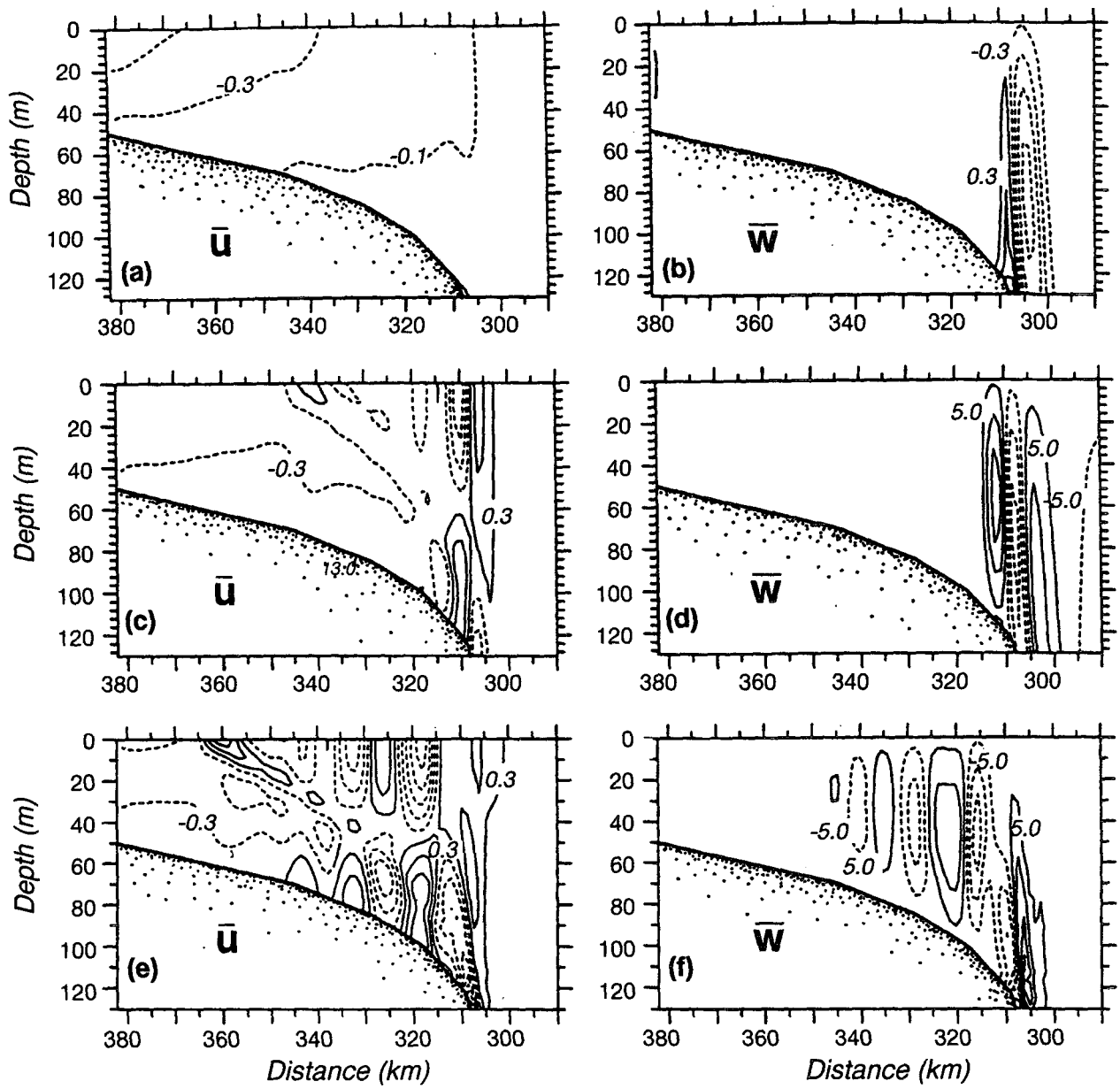

FIG. 6. Structure of residual cross-bank current ($\bar{u}$) and vertical velocity ($\bar{w}$) in the upper 130 m on the southern flank for the homogeneous (a and b), winter (c and d), and summer (e and f) stratification cases. The contour interval of $\bar{u}$ is 0.2 cm s^{-1} for the homogeneous case and 0.6 cm s^{-1} for the stratified cases. The contour interval of $\bar{w}$ is 0.6×10^{-3} cm s^{-1} for the homogeneous case and 10×10^{-3} cm s^{-1} for the stratified cases.

face pressure gradient can generate a southwestward geostrophic current of about 0.1 cm s^{-1} in the homogeneous case, 0.3 cm s^{-1} in winter, and 0.7 cm s^{-1} in summer. The negative mean surface pressure gradient found at the edge of the northern flank is about 0.3×10^{-6} in the homogeneous case, 0.8×10^{-6} in winter, and 1.0×10^{-6} in summer. Correspondingly, the northeastward geostrophic current associated with this negative pressure gradient is about 3 cm s^{-1} in the homogeneous case, 8 cm s^{-1} in winter, and 10 cm s^{-1} in summer.

Figure 9 shows the cross-bank distribution of the mean eddy viscosity $\bar{K}_m$ for the homogeneous, winter, and summer stratification cases. In the homogeneous case (Fig. 9a), the predicted $\bar{K}_m$ is characterized with a parabolic curve in the vertical on the top of the bank and quickly decreases in magnitude away from the bank. The maximum $\bar{K}_m$ is about 0.06 m^2 s^{-1} on

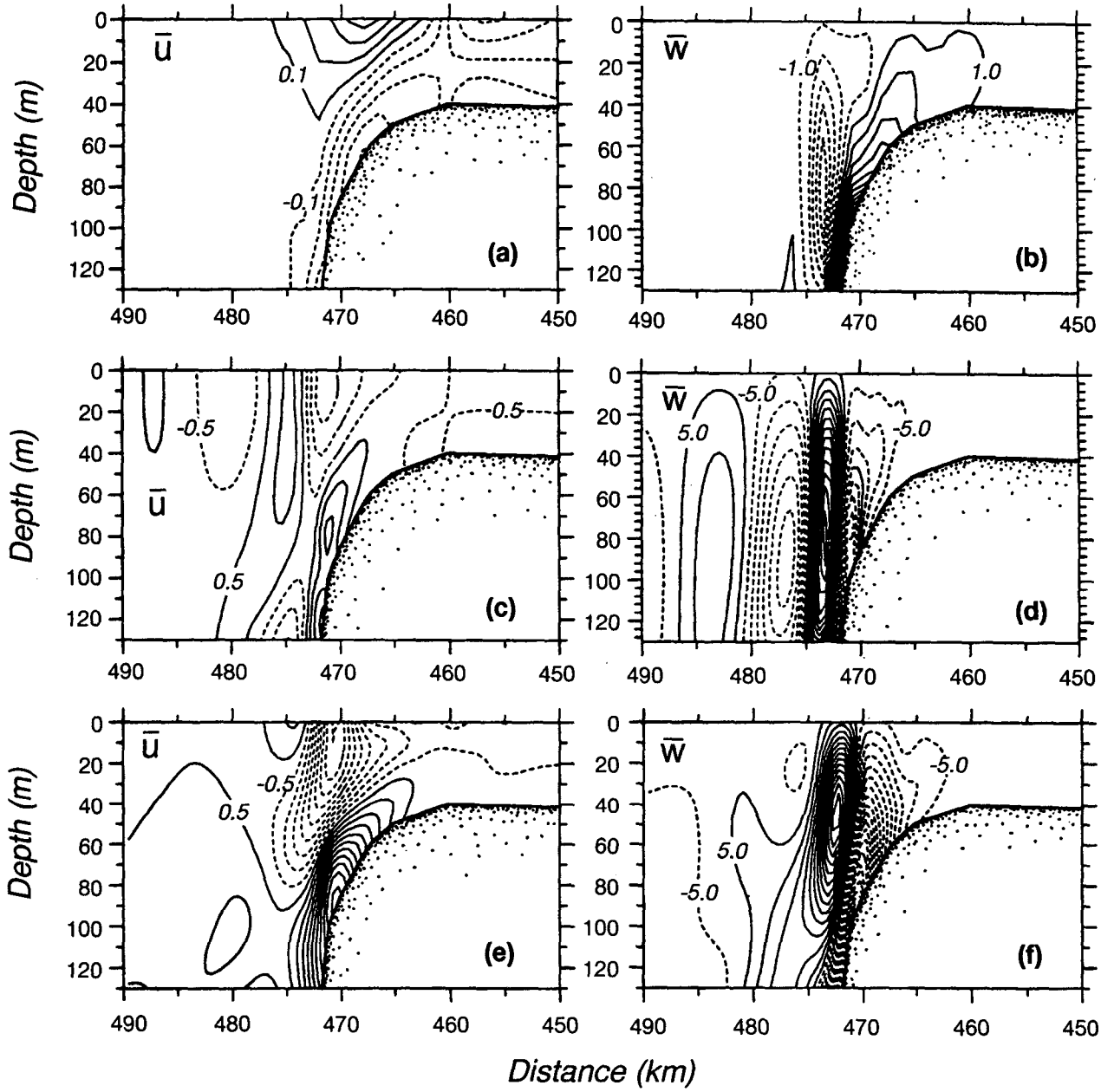

FIG. 7. Structure of residual cross-bank current ($\bar{u}$) and vertical velocity ($\bar{w}$) in the upper 130 m on the northern flank for the homogeneous (a and b), winter (c and d), and summer (e and f) stratification cases. The contour interval of $\bar{u}$ is 0.2 cm s for the homogeneous case and 1.0 cm s^{-1} for the stratified cases. The contour interval of $\bar{w}$ is 2.0×10^{-3} cm s^{-1} for the homogeneous case and 10×10^{-3} cm s^{-1} for the stratified cases.

the top of the bank and at a depth of 120 m over the slope on the northern flank but only 0.02 m^2 s^{-1} at the edge of the southern flank. In winter (Fig. 9b), the distribution of $\bar{K}_m$ remains unchanged on the top of the bank where the water is vertically well mixed, but it is significantly reduced over the steep sloping sides of the bank where the water is weakly stratified. The reduction of $\bar{K}_m$ over the slope is much larger as stratification is increased in summer (Fig. 9c).

4. Comparison with observations

a. Comparison with tidal current observations

It is difficult to make simple comparisons between the predicted and observed tidal currents over Georges Bank because of the varying influence of the seasonal stratification cycle and the strictly two-dimensional nature of our numerical model. Most measurements of M_2 tidal currents over Georges Bank were made

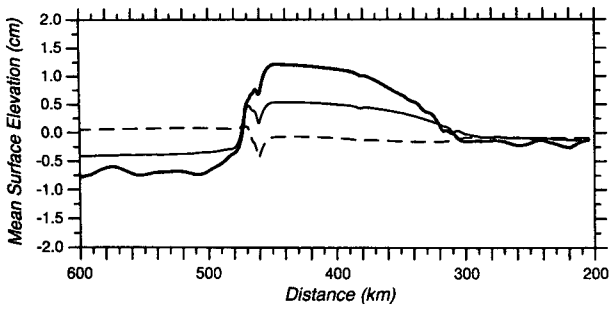

FIG. 8. Distribution of the mean cross-bank surface elevation for homogeneous (dashed line), winter (solid line), and summer (heavy solid line) stratification cases.

during time periods of about 2–60 days (Moody et al., 1984; Marsden 1986; Loder et al., 1992), where the temporal variability of the internal tide was included. For this reason, our comparison with tidal observations will be limited to barotropic cases where the observed tidal currents were obtained either by averaging over all seasons or in the vertically well-mixed region. Measurements fitting this condition have been made at two sites on the southern flank, stations A at the 85-m isobath and station K at the 61-m isobath, and one site on the northeast top of the bank, station P3 at the 45-m isobath (Fig. 3). Figure 10 shows the vertical structure of the predicted and observed M_2 tidal currents at these three stations. The amplitudes of predicted along- and cross-bank tidal currents are in reasonable agreement with observations at stations A and K within measurement uncertainty, but about 6–10 cm s^{-1} less at station P3. A region of maximum current amplitude of about 90–110 cm s^{-1} in the cross-bank direction is found near station P3, 60 km east of our model section (Moody et al., 1984; Loder et al., 1992), suggesting that the relatively large difference between model and observed results on the northern side of Georges Bank is probably due to the spatial variation of tidal currents there. Overall, this limited comparison between model-predicted and observed M_2 currents across the bank is encouraging.

b. *Comparison with observations of the tidal mixing fronts*

The predicted seasonal variability in the strength and location of tidal mixing fronts with winter and summer stratification is in good agreement with observations. In summer, the model predicts the well-defined tidal-induced thermal fronts at both the 40-m isobath on the northern flank and the 60-m isobath on the southern flank. As stratification lessens in winter, the tidal mixing front on the southern flank moves toward the shelf break, while the tidal front on the northern flank weakens in intensity but remains almost fixed in position. These model results agree well with existing observations of the tidal mixing fronts shown in Fig. 2. In addition to increased atmospheric cooling and wind mixing in winter, the disappearance of the tidal mixing front on the southern flank during winter can also be interpreted as the offshore migration of the tidal front predicted on the southern flank for weak stratification. As the tidal mixing front moves to the shelf break, it merges with the shelf/slope front there, resulting in a single frontal structure on the southern flank. This result suggests an intensification of the shelf/slope front due to interaction with the tidal mixing front during winter since both fronts have similar density structures.

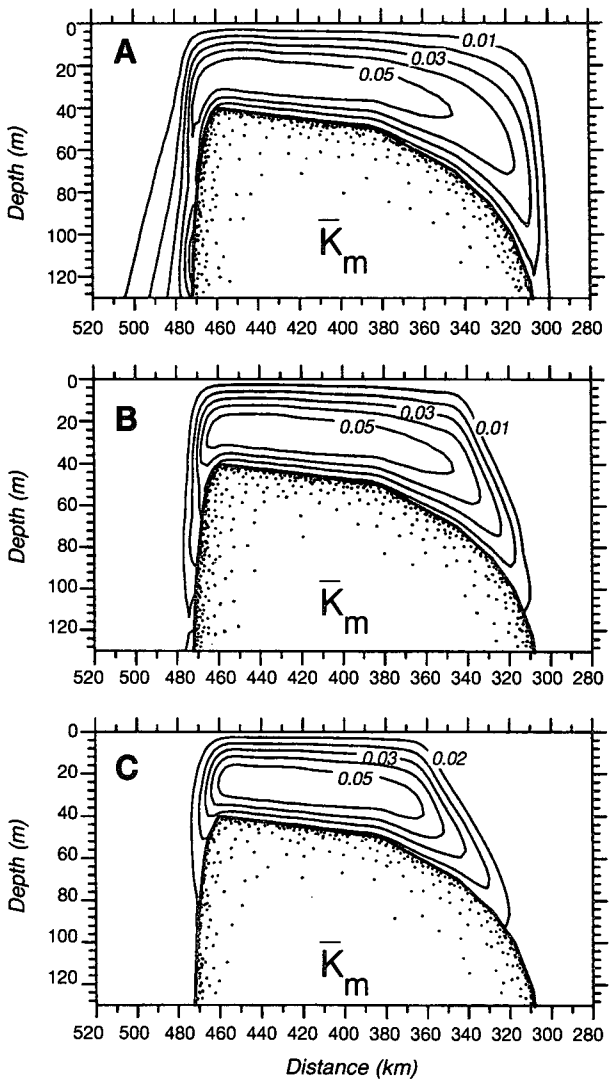

FIG. 9. Distribution of the mean vertical eddy viscosity $\bar{K}_m$ across the bank for homogeneous (a), winter (b), and summer (c) stratification cases. The contour interval of $\bar{K}_m$ is 0.01 m^2 s^{-1}.

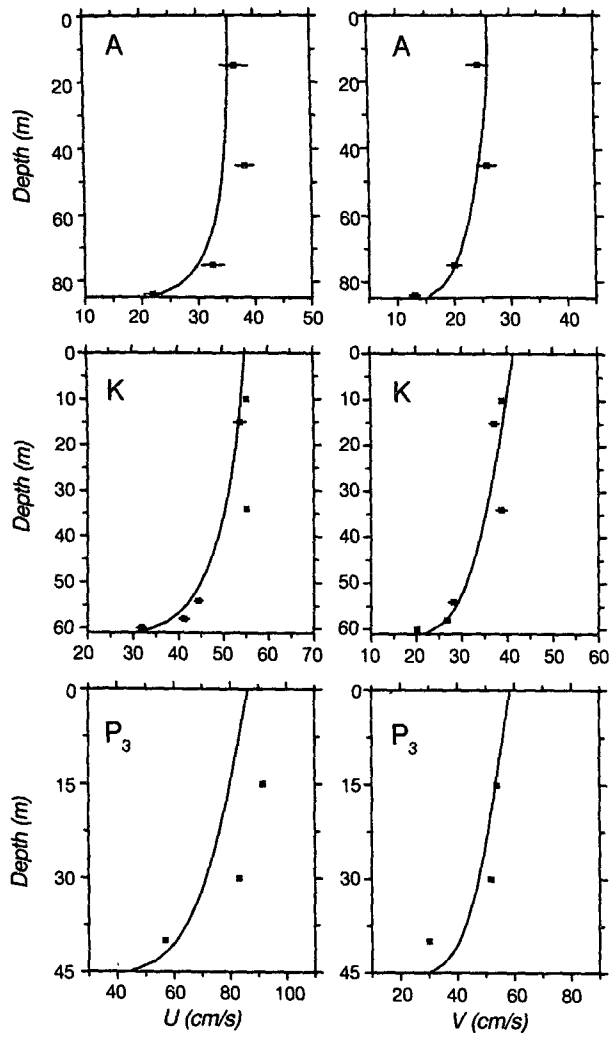

FIG. 10. Comparison between amplitudes of the predicted and observed tidal currents at stations A, K, and P3. The solid line is the predicted tidal current component. The symbol * is an individual tidal current datum at stations A, K, and P3.

TABLE 1. Comparison between observed and predicted along-bank mean currents during winter. H is the water depth; Z_m is the measurement depth; $\bar{v}_0$ is the observed mean current plus standard deviation; $\bar{v}_b$ and $\bar{v}_w$ are the model-predicted mean currents for the homogeneous and weak stratification cases.

			Observation	Homogeneous case	Winter case
Station	H (m)	Z_m (m)	$\bar{v}_0$ (cm s^{-1})	$\bar{v}_b$ (cm s^{-1})	$\bar{v}_w$ (cm s^{-1})
A	85	45	2 ± 3–8 ± 8	1.1	2.1
		75	1 ± 3–7 ± 7	0.8	1.1
		84	1 ± 3–5 ± 5	0.6	0.7
M2	85	10	−19 ± 10	−17.4	−26.8
		44	none	−14.6	−18.1
		77	−8 ± 7	−8.4	−9.6
M1	200	10	−15 ± 13	−0.2	−1.7
		77	−5 ± 10	−0.2	−2.9
		192	−2 ± 8	−0.1	−0.8

c. *Comparison with wintertime observed along-bank mean current*

The wintertime mean Eulerian current measurements clearly show a southwestward flow with a speed of about 5 cm s^{-1} at a depth of 45 m at station A on the southern flank, and northeastward flow with a speed of about 19 cm s^{-1} near the surface at station M1 on the northern flank (Fig. 3 and Table 1). Butman et al. (1983) estimated that only about 40% of the along-bank mean flow (about 2 cm s^{-1}) at a depth of 45 m at station A was driven by tidal rectification during winter. A similar circulation pattern is also predicted by our numerical model for the homogeneous and weakly stratified cases. In the homogeneous case, the model predicts a southwestward mean flow of about 1.1 cm s^{-1} at a depth of 45 m at station A on the southern flank and a northwestward mean flow of about 17.4 cm s^{-1} near the surface at station M2 on the northern flank. As weak stratification is included, the along-bank mean flow increases to about 2.1 cm s^{-1} at station A and about 26.9 cm s^{-1} at station M2. Since stratification differed during the different measurement periods, the real currents should vary within the homogeneous and weakly stratified cases during winter. Considering the relatively large variations in the measurements, we conclude here that the model predictions

TABLE 2. Comparison between observed and predicted along-bank mean currents during summer. H is the water depth; Z_m is the measurement depth; $\bar{v}_0$ and $\bar{v}_s$ are the observed and predicted currents plus standard deviations during summer.

			Observation	Summer case
Station	H (m)	Z_m (m)	$\bar{v}_0$ (cm s^{-1})	$\bar{v}_s$ (cm s^{-1})
A	85	15	8 ± 5–17 ± 9	3.8
		45	10 ± 6–13 ± 7	3.3
		75	2 ± 2–4 ± 5	0.5
		84	1 ± 2–3 ± 2	0.2
M2	85	10	−30 ± 9–−33 ± 8	−27.5
		44	−19 ± 5–−29 ± 8	−21.0
		77	−6 ± 6–−9 ± 5	−11.5
M1	200	10	−3 ± 7–−27 ± 11	−3.4
		77	−5 ± 5–−7 ± 4	−3.8
		192	−2 ± 3–−2 ± 6	−0.3
MS2	45	15	−13.4 ± 0.7	−14.1
		30	−7.9 ± 0.5	−11.7

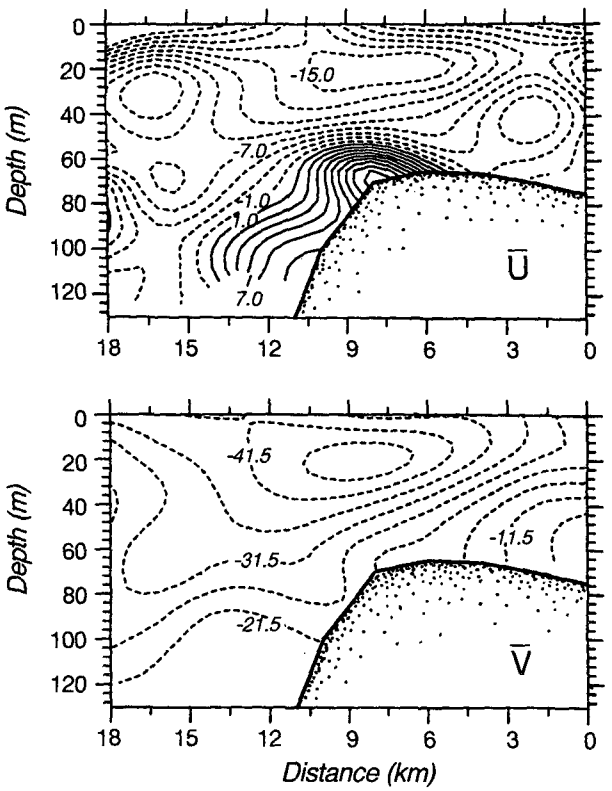

FIG. 11. Distribution of cross- (upper) and along- (lower) bank residual currents along the CTD/ADCP section L made in 1988 on the northern edge of Georges Bank by Loder et al. (1992). The negative along-bank residual current is eastward, and negative cross-bank residual current is toward the bank. The contour interval is 2.0 cm s^{-1} for the cross-bank residual current and 5.0 cm s^{-1} for the along-bank residual current. The location of section L is shown in Fig. 3.

of along-bank mean current in winter agree reasonably well with observations.

d. Comparison with summertime observed along-bank mean current

Summertime observations show an intensified clockwise circulation around the bank, flowing southwestward with a speed of about 8–17 cm s^{-1} at a depth of 15 m at station A on the southern flank and northeastward with a speed of 30 to 33 cm s^{-1} and 3 to 27 cm s^{-1} at a depth of 10 m at stations M2 and M1 on the northern flank, respectively (Fig. 3 and Table 2). Long-term current measurements conducted by Marsden (1986) show northeastward flow of 13.4 ± 0.7 cm s^{-1} at a depth of 15 m at station MS2 (Table 2). The numerical model also predicts an intensified near-surface clockwise-like circulation in summer: the model shows a southwestward flow of about 3.8 cm s^{-1} at a depth of 15 m at station A on the southern flank and a near-surface northeastward flow of about 14 cm s^{-1}, 27 cm s^{-1}, and 3 cm s^{-1} at stations MS2, M2, and M1 on the northern flank, respectively.

Extensive CTD, ADCP, and moored current meter measurements were made over the northern flank under light wind conditions by Loder et al. (1992) during 2–3 July 1988 (see Fig. 3 for the location of their measurement section). They observed a strong tidal current on the northern flank with a maximum amplitude of 110 cm s^{-1} in the cross-bank direction and 70 cm s^{-1} in the along-bank direction. Associated with the strong tidal current and stratification, both the ADCP and moored current meter data consistently showed a strong northeastward along-bank mean current on the northern flank with a maximum of about 50 cm s^{-1} at a depth of 20 m near the shelf break (see Fig. 11, lower panel). Although this observed section is about 60 km east of our model section where the maximum cross-bank tidal current is only about 90 cm s^{-1}, the structure of the observed along-bank flow is quite similar to our model results.

Lagrangian current measurements made with satellite-tracked drifters with drogues centered at 5 m during the 1989 South Channel Ocean Productivity Experiment survey (Limeburner and Beardsley 1989) exhibited continuous drifter trajectories around Georges Bank during summer, with a mean speed of about 1–20 cm s^{-1} on the southern flank and about 20–45 cm s^{-1} on the northern flank. Theory suggests that the tidally rectified Lagrangian mean current is generally less than the Eulerian mean current because of a Stokes velocity component over the variable bottom slope (Loder 1980; Zimmerman 1978, 1980, 1981). With a barotropic harmonic truncation model, Loder (1980) estimated that the Lagrangian mean current is only about two-thirds of the mean Eulerian current. However, if a density front is included, the Lagrangian mean current may approach the Eulerian current (Loder and Wright 1985). If this is true in our case, the model-predicted mean current is in reasonable agreement with the observed Lagrangian mean current on the northern flank of the bank. The big difference between the observed Lagrangian and predicted Eulerian along-bank residual currents on the southern flank is probably due to processes not included in the model, especially those associated with the shelf/slope front, and surface and lateral buoyancy forcing.

e. Comparison with wintertime cross-bank mean current

Observations show opposite cross-bank mean circulation patterns over the two sides of Georges Bank during winter. On the southern flank, the water at station A tends to flow off bank with a speed of 0.5 to 1.0 cm s^{-1} above 75 m and on bank at the same speed near the bottom. On the northern flank, however, the water at stations M2 and M1 tends to flow on bank

TABLE 3. Comparison between the observed and predicted cross-bank mean currents during winter; H is the water depth; Z_m is the measurement depth; $\bar{u}_0$ is the observed cross-bank mean current plus standard deviation; $\bar{u}_b$ and $\bar{u}_w$ are the model-predicted barotropic and weakly stratified mean currents.

Station	H (m)	Z_m (m)	Observation $\bar{u}_0$ (cm s^{-1})	Homogeneous case $\bar{u}_b$ (cm s^{-1})	Winter case $\bar{u}_w$ (cm s^{-1})
A	85	45	−0.5 ± 3.0	−0.22	−0.29
		75	−1.0 ± 3.0	−0.07	0.05
		84	1.0 ± 2.0	−0.02	0.15
M2	85	10	−1.3 ± 4.2	−0.36	−2.48
		44	none	−0.09	0.11
		77	4.8 ± 3.2	−0.66	1.50
M1	200	10	−0.5 ± 6.5	0.04	−0.79
		77	−2.1 ± 3.8	0.01	−0.14
		192	2.0 ± 3.0	−0.07	0.55

with a speed of 0.5 to 1.3 cm s^{-1} near the surface and off bank with a speed of 2.0–4.8 cm s^{-1} near the bottom (Table 3). This circulation pattern is consistent with our model results for the weakly stratified case, which shows an offbank flow of about 0.3 cm s^{-1} near the surface and an on-bank flow of 0.1–0.2 cm s^{-1} near the bottom at station A, and an onbank flow of about 0.1 to 2.5 cm s^{-1} near the surface and an offbank flow of about 0.5–1.5 cm s^{-1} near the bottom at stations M2 and M1.

f. Comparison with summertime cross-bank mean current

On the southern flank, the model predicts an onbank flow of 0.5 cm s^{-1} near the surface and an offbank flow of 0.03 to 0.43 cm s^{-1} near the bottom at station A, in good agreement with observations considering the uncertainty of the measurements (Table 4). On the northern flank, at station M2, the model shows an on-bank flow of 9.0 cm s^{-1} at a depth of 10 m near the surface and an offbank flow of 13 cm s^{-1} at a depth of 77 m near the bottom, in good comparison with observation in both magnitude and direction (Table 4). A similar vertical structure was found by Loder et al. (1992) at section L. Both moored current meter and ADCP data show an onbank mean flow in the upper 70 m and an offbank return mean flow in the lower 80 m above the bottom with a maximum velocity of about 10 cm s^{-1} near the surface and bottom (see Fig. 11, upper panel). In addition, on the top of the bank where the water is vertically well mixed, the model shows that the water tends to flow southward at all depths with a speed of about 0.1 to 0.6 cm s^{-1}, consistent with the current meter data taken by Marsden (1986), who reported a southward flow at all depths of about 0.7 to 3.2 cm s^{-1} at the 40-m isobath.

5. Diagnostic analysis for dynamic balances

A diagnostic analysis of the mean momentum and heat balances has been made for both the homogeneous and summer stratification cases, and the resulting cross-bank distribution of dominant terms is shown in Figs. 12–13. Unlike the symmetric bank case discussed in Part I, the mean momentum balance in the homogeneous case is asymmetric, reflecting the asymmetry in the topography. On the southern flank, the mean momentum is balanced among horizontal advection, the Coriolis term, and vertical friction in both cross- and along-bank directions. On the northern flank, however, steep bottom topography leads to a much larger surface pressure gradient in the cross-bank direction and larger horizontal advection and vertical friction in the along-bank direction, so that the momentum is primarily balanced among the horizontal advection, the Coriolis term, and surface pressure gradient in the cross-bank direction and between the horizontal advection and vertical friction in the along-bank direction (Fig. 12). This asymmetry suggests that the Coriolis term in the along-bank momentum equation is important only over the southern flank where the bottom slope is smaller and the along-bank horizontal advection is weaker, and also the mean surface pressure gradient tends to increase as the bottom slope is steeper. These results are consistent with previous analytical and numerical results for vertically averaged or depth-dependent models (Loder 1980; Greenberg 1983; Loder and Wright 1985) and diagnostic results for a symmetric bank (Part I).

The momentum balance in the summer stratification case is very complicated. All dynamical terms ex-

TABLE 4. Comparison between the observed and predicted cross-bank mean currents during summer; H is the water depth; Z_m is the measurement depth; $\bar{u}_0$ is the observed current plus standard deviation; and $\bar{u}_s$ is predicted current during summer.

Station	H (m)	Z_m (m)	Observation $\bar{u}_0$ (cm s^{-1})	Summer case $\bar{u}_s$ (cm s^{-1})
A	85	15	1 ± 3–4 ± 5	0.53
		45	1 ± 3–5 ± 8	0.16
		75	−1 ± 1–−2 ± 3	−0.43
		84	1 ± 1–2 ± 2	−0.03
M2	85	10	−3 ± 5–−5 ± 6	−9.25
		44	−2 ± 6–−6 ± 4	−1.44
		77	5 ± 3–−11 ± 4	12.85
M1	200	10	−1 ± 8–−2 ± 6	0.34
		77	−1 ± 3–2 ± 3	0.99
		192	−1 ± 3–1 ± 5	−4.88
MS2	45	15	−1.4 ± 1.1	−1.3
		30	2.2 ± 0.8	0.7
		40	−1.3	−0.1

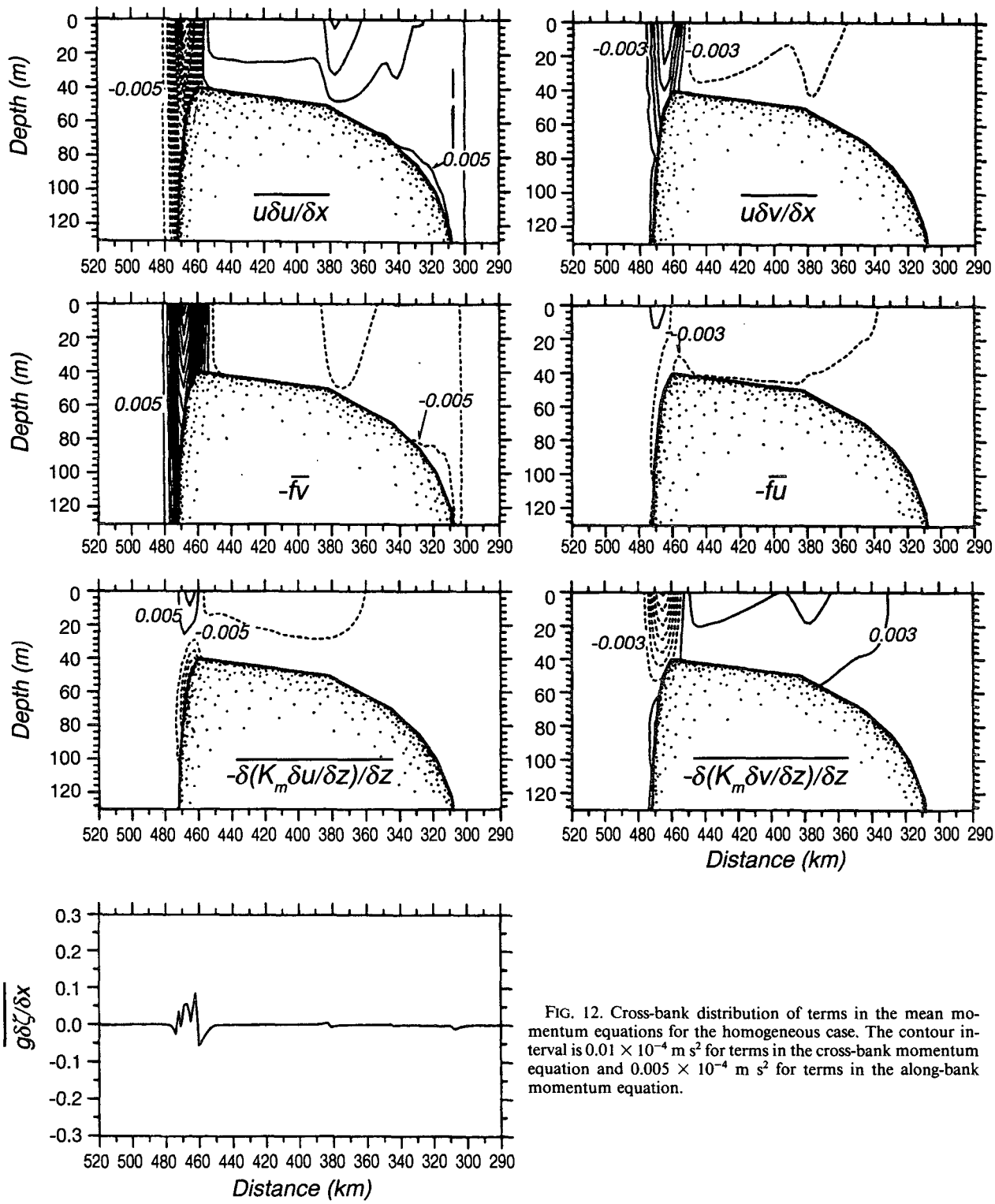

FIG. 12. Cross-bank distribution of terms in the mean momentum equations for the homogeneous case. The contour interval is 0.01×10^{-4} m s^2 for terms in the cross-bank momentum equation and 0.005×10^{-4} m s^2 for terms in the along-bank momentum equation.

cept the cross-bank vertical friction term become important in the cross- and along-bank momentum balances over Georges Bank during summer (Fig. 13). Associated with the reduction in $\bar{K}_m$ and increase in vertical shears due to stratification, the vertical friction term

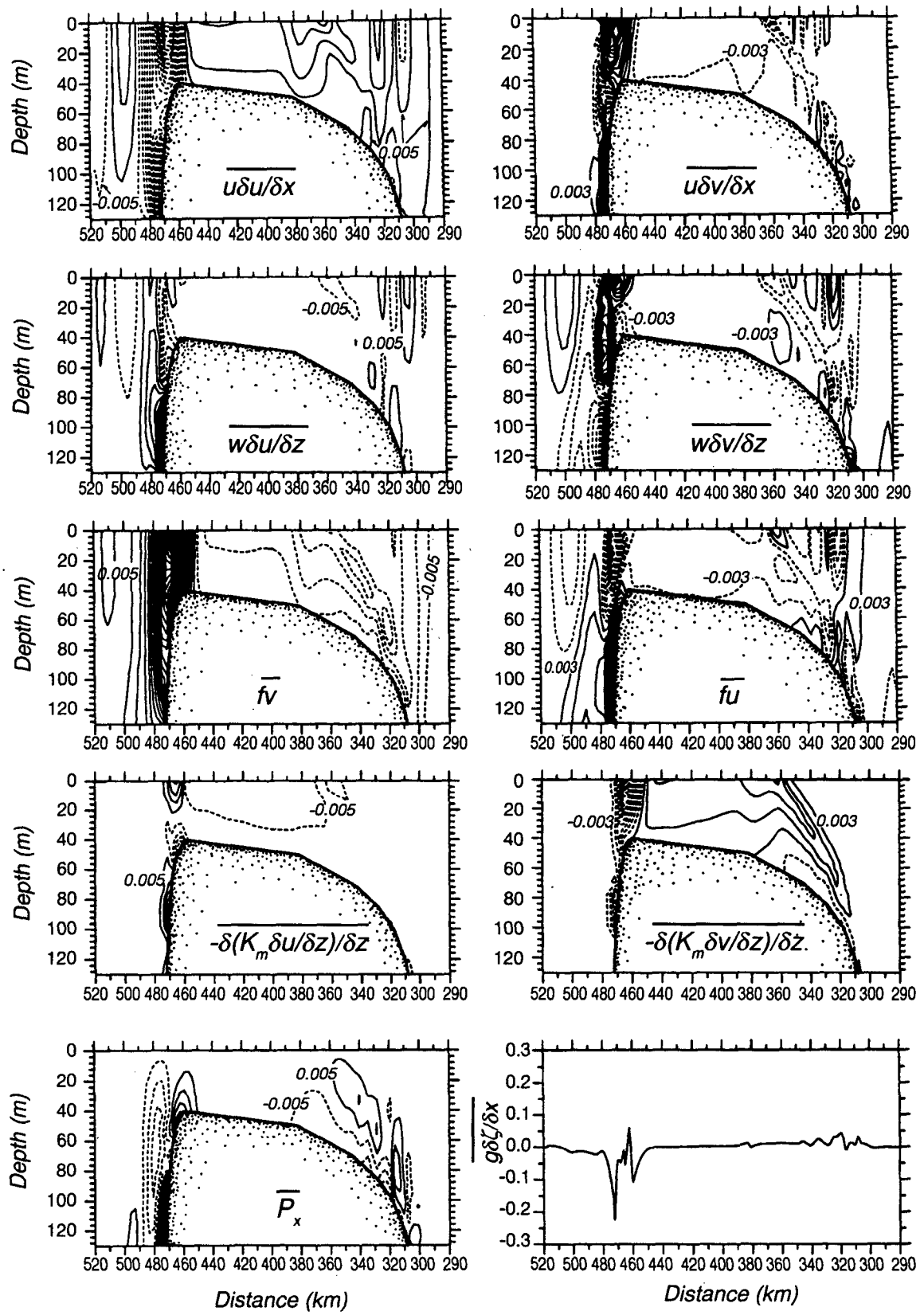

FIG. 13. Cross-bank distribution of terms in the mean momentum equations for the summer stratification case. The contour interval is 0.01×10^{-4} m s^2 for terms in the cross-bank momentum equation and 0.005×10^{-4} m s^2 for terms in the along-bank momentum equation.

$$\overline{\frac{\partial}{\partial z}\left(K_m \frac{\partial v}{\partial z}\right)}$$

in the along-bank direction is significantly increased on both sides of the bank during summer. The maximum of

$$\overline{\frac{\partial}{\partial z}\left(K_m \frac{\partial v}{\partial z}\right)}$$

is only about -0.04×10^{-4} m s^2 on the northern flank and 0.01×10^{-4} m s^2 on the southern flank in the homogeneous case but it increases to -0.09×10^{-4} m s^2 on the northern flank and 0.02×10^{-4} m s^2 on the southern flank in summer. The increase of vertical friction due to stratification strengthens the stratified tidal rectification and hence increases the residual currents over the bank. In addition to the generation of a relatively strong baroclinic pressure gradient due to tidal mixing, the nonlinear interaction between the barotropic and internal tidal currents and internal tidal currents themselves increases as stratification increases. The cross-bank horizontal advection, which has a single maximum of about 0.3×10^{-5} m s^2 on the southern flank or about 0.2×10^{-4} m s^2 on the northern flank in the homogeneous case, is characterized by multiple cells on both flanks of the bank in summer and its magnitude increases to 0.8×10^{-5} m s^2 on the southern flank and 0.4×10^{-4} m s^2 on the northern flank. Similar results can be seen in the other nonlinear terms in both cross- and along-bank momentum equations, implying a complex nonlinear driving mechanism for stratified tidal rectification over Georges Bank.

Similar to the results on a symmetric bank (Part I), the mean temperature balance is relatively simple near tidal mixing fronts on both sides of Georges Bank. Since vertical thermal diffusion is in general one or two orders of magnitude weaker than the advective terms in the heat equation, the mean temperature field is maintained through a basic balance between horizontal and vertical temperature advection (Fig. 14).

The relative contributions of the tidal mixing fronts and nonlinear interaction between stratified tidal currents to the intensification of along-bank residual flow is estimated here using a simple scale analysis. On the southern flank, the horizontal and vertical advection terms associated with nonlinear interaction between stratified tidal currents are mainly characterized by a first mode structure in the vertical, with a maximum at the surface and bottom, respectively. As an example, at the 84-m isobath on the southern flank, maxima of the horizontal and vertical advection terms at the surface in the summer case are $(\overline{u\,\partial u/\partial x})_s = -0.03 \times 10^{-4}$ m s^2, $(\overline{w\,\partial u/\partial z})_s = 0.03 \times 10^{-4}$ m s^2, which are the same in magnitude but opposite in sign and tend to cancel each other. On the other hand, the maximum

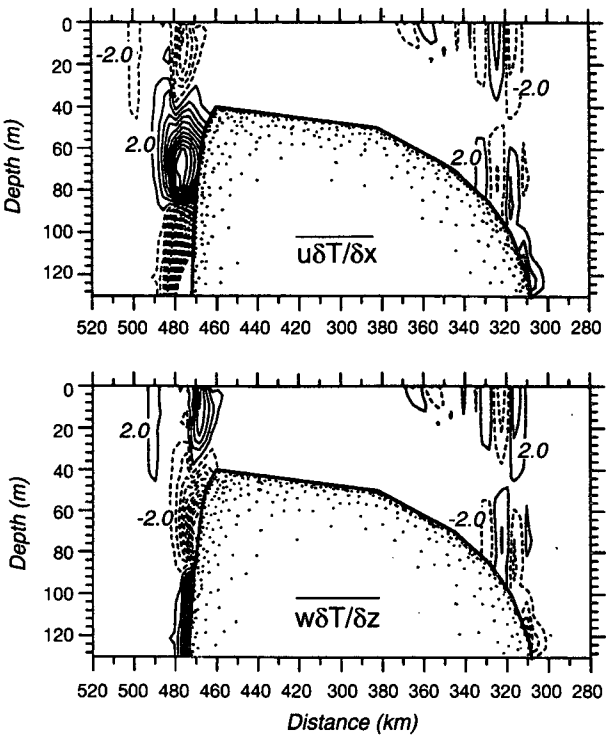

FIG. 14. Cross-bank distribution of terms in the heat equation for the summer stratification case. The contour interval is 0.2×10^{-4} °C s^{-1} for heat fluxes.

baroclinic pressure gradient associated with the tidal mixing front on the southern flank is $\overline{\partial P/\partial x} = 0.03 \times 10^{-4}$ m^2 s^{-1}, which coincides with the axes of the maximum along-bank residual current, suggesting that the density gradient is responsible for the summertime intensification of along-bank residual current on the southern flank.

On the northern flank, at the place where the maximum along-bank residual flow is located, both of the horizontal and vertical advection terms are negative and tend to increase the along-bank residual flow. The maximum horizontal advection in the cross-isobath direction is given by

$$\left(\overline{u\frac{\partial u}{\partial x}}\right)_h = -0.24 \times 10^{-4} \text{ m s}^2$$

for the homogeneous case and

$$\left(\overline{u\frac{\partial u}{\partial x}}\right)_s = -0.37 \times 10^{-4} \text{ m s}^2$$

for the summer case. Thus, the mean baroclinic horizontal advection associated with stratified tidal rectification on the northern flank can be estimated as

$$\left(\overline{u\frac{\partial u}{\partial x}}\right)_b = \left(\overline{u\frac{\partial u}{\partial x}}\right)_s - \left(\overline{u\frac{\partial u}{\partial x}}\right)_h = -0.13 \times 10^{-4} \text{ m s}^2.$$

However, the mean baroclinic pressure gradient associated with the tidal mixing front there is only equal to $\overline{\partial P}/\partial x = -0.003 \times 10^{-4}$ m^2 s^{-1}, which is two orders of magnitude smaller than the mean horizontal advection. Therefore, the stratified tidal rectification associated with the nonlinear interaction between the barotropic and internal tidal currents and internal tidal currents themselves is more important for the summertime intensification of along-bank residual current on the northern flank.

Possible driving mechanisms for the cross-bank residual current are discussed next. On the southern flank, the close similarity between the structure of cross-bank residual flow and horizontal and vertical advection implies a driving mechanism of cross-bank mean flow due to stratified tidal rectification associated with nonlinear interaction between tidal currents. Maas and Zimmerman (1989a,b) analytically studied stratified tidal rectification over small amplitude bottom topography and found that nonlinear interaction between tidal currents over the shelf generates three cross-bank residual circulation cells with a horizontal scale of $2l_0$–$4l_0$ ($l_0 = U/\omega$, the barotropic tidal current excursion). Since the bottom slope is relatively small over the top of Georges Bank, their theory may be used to help interpret the multiple cell structure of cross-bank residual current found over the shelf region on the southern flank. The barotropic tidal current excursion is about 3.5 km for a tidal current of about 50 cm s^{-1} over the shelf, so that the horizontal scale of the cross-bank circulation cell caused by the M_2 internal tides should be about 7–14 km. The model-predicted cross-bank circulation cell on the southern flank has a horizontal scale of about 10 km in summer, which is in good agreement with the analytical solution. Using a fourth-order Runge-Kutta shooting method, we can also estimate the wavelength of the M_2 internal tide from the inferred vertical temperature structure. The wavelength of the first baroclinic mode is about 15 km near the southern flank and decreases as the wave propagates onto the bank, thus supporting our argument on the driving mechanism of nonlinear tidal interaction for the cross-bank circulation on the southern flank. The spatial distribution and strength of the multiple circulation cells found on the southern flank may be associated with the spatial distribution of temperature in which the tidal mixed layer is dominant near the bottom and increases as the water becomes shallower. Tidal mixing and bottom stress tend to dissipate the internal tidal energy as the wave propagates onto the bank, and hence reduces the strength and vertical scale of the circulation cell as the water becomes shallower.

The driving mechanism for a single cross-bank circulation cell on the northern flank is apparently more complex since all dynamical terms are relatively strong there. Based on the balance between the surface pressure gradient and bottom friction in the bottom boundary layer, Loder (1980) suggested that a bottom flow can be driven in the $-x$ (onbank) direction by the positive unbalanced cross-bank surface pressure gradient against the bottom friction and, in turn, in the $+x$ (offbank) direction by the negative surface pressure gradient. Although the cross-bank circulation pattern on the northern flank is consistent with Loder's (1980) suggestion, the momentum balance near the bottom is more complicated than the simple relation Loder (1980) proposed. Wright and Loder (1985) also found in a depth-dependent barotropic model a complex momentum balance in the bottom boundary layer. Two reference points in the cross-bank circulation cell on the northern flank are taken here to examine the momentum balance in the stratified bottom boundary layer on the northern flank (see Fig. 15). At the 85-m isobath, both Coriolis force and vertical friction in the cross-bank direction are positive near the bottom; they are balanced by surface and baroclinic pressure gradients and horizontal advection. In the along-bank direction, the vertical friction is only half of the Coriolis force so that nonlinear interaction becomes more important in the along-bank momentum balance in the bottom boundary layer. At the 140-m isobath, however, relatively strong stratification results in weak vertical friction in both along- and cross-bank directions throughout the water column. The momentum balance is then mainly between surface and baroclinic pressure gradients plus corrections due to the net contribution of horizontal and vertical advection and Coriolis force in the cross-bank direction, and between Coriolis force and the difference of horizontal and vertical advection in the along-bank direction. Relatively large nonlinear terms and baroclinic pressure gradient suggest that tidal mixing and stratified tidal nonlinear interaction are both important for the formation of the cross-bank circulation cells on the northern flank during summer, where Ekman theory is no longer valid as stratification is added.

6. Conclusions

Homogeneous and stratified tidal rectification over an idealized Georges Bank has been studied using a two-dimensional version of the Blumberg and Mellor (1987) numerical ocean circulation model. The model physics includes primitive equations in the horizontal direction, the hydrostatic approximation in the vertical, and the Mellor and Yamada (1982) level 2½ turbulent closure model to simulate turbulent friction and mixing. The model domain consists of a vertical slice running roughly northwest across the center of Georges Bank, and the flow is forced by a simple elevation variation imposed at the southeast open boundary of the model with the period of the dominant M_2 tide (12.42 h).

In the homogeneous case, the model predicts a topographically controlled residual circulation over the

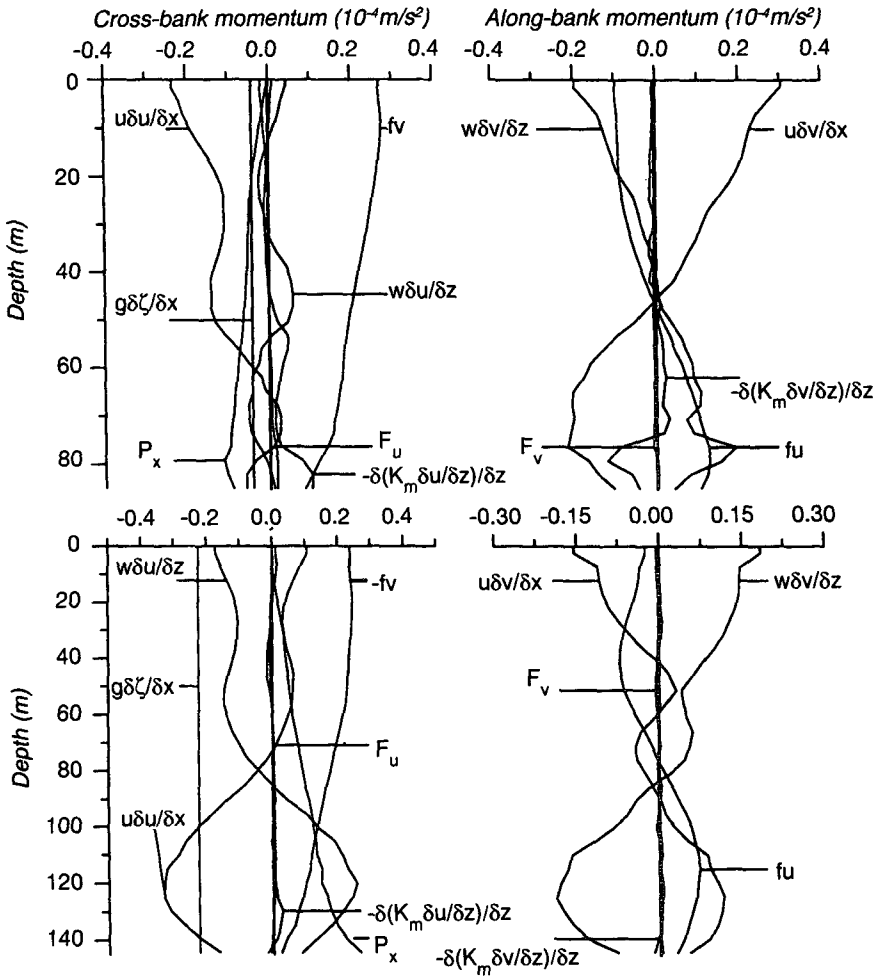

FIG. 15. The vertical profile of individual terms in the mean cross- and along-bank momentum equations at the 85-m and 145-m isobaths on the northern flank for the summer stratification case.

bank, flowing northeastward as a strong surface-intensified jet with a maximum speed of about 16 cm s^{-1} along the northern flank, and southwestward as a relatively weak and broader current with a maximum of about 3 cm s^{-1} from the top of the bank to the southern flank. The cross-bank circulation is mainly characterized by a single circulation cell on both the southern and northern flanks. As stratification is added, stratified tidal rectification and tidal mixing intensify along- and cross-bank residual currents and hence modify the vertical structure of the residual flow. In the summer stratification case, the tidal front is located at about the 40-m isobath on the northern edge of the bank and at the 50–60-m isobath on the southern flank, about 70–80 km onbank from the shelf break. This results in an intensification of the along-bank residual current with a maximum of about 32 cm s^{-1} on the northern flank and about 8 cm s^{-1} on the southern flank. In the winter stratification case, the position of the tidal front remains relatively fixed on the northern flank; however, it moves to the shelf break on the southern flank. The winter maximum of along-bank residual flow is about 26 cm s^{-1} on the northern flank and about 6 cm s^{-1} at the shelf break on the southern flank. The numerical model results are consistent with existing theories for stratified tidally rectified flow and observations of mean flow. The predicted along-bank residual current is relatively weaker than observed on the southern flank during summer, suggesting that buoyancy driving associated with the shelfbreak front and the surface heat flux is also important in generating the residual flow observed on the southern flank.

Additional dynamic mechanisms become active in stratified tidal rectification. In the homogeneous case, the residual current is generated by the nonlinear transfer of momentum fluctuations from tidal currents to the mean flow. When stratification is included, a tidal-induced front due to turbulent mixing, internal

tidal generation over the slope, and modified internal friction due to stratification all play important roles in modifying the strength and distribution of residual currents over the bank. On the southern flank, density-driving associated with the tidal mixing front is critically important for intensification of the along-bank residual flow, while stratified tidal nonlinear interaction plus tidal mixing are responsible for the cross-bank multiple cell circulation pattern found over the southern shelf. On the northern flank, however, stratified tidal nonlinear interaction plays a more important role in increasing the maximum along-bank mean flow than the baroclinic density gradient due to the tidal mixing front. Also, the cross-bank residual current on the northern flank is mainly driven by nonlinear advection and surface and baroclinic pressure gradients while Ekman theory is no longer valid in the bottom boundary layer.

Our numerical experiments do not include the buoyancy- and wind-driven circulations caused by wintertime surface cooling and wind mixing, nor do they include the thermohaline circulations generated by either tidal mixing of the salinity field on either flank of the bank or that associated with the shelf/slope front. Wintertime surface cooling can also mix water vertically over the top of the bank, generating density fronts on both sides of the bank. The study of the nonlinear interaction between tidal mixing and convective overturning on residual currents should be very interesting. Wind mixing can create a surface mixed layer over the slope and in the deep region, which may modify the spatial distribution and transport of along-bank mean flow. The seasonal variation of freshwater input around the bank may also cause a corresponding variation in the strength of the salinity fronts and cross-bank density gradients and thus influence the strength and distribution of residual currents over the bank. We hope to use both two- and three-dimensional versions of the numerical model to tackle these questions in future research.

Acknowledgments. This research was supported by the National Science Foundation under Grants OCE 87-13988 and OCE 91-01034 and by the National Center for Atmospheric Research under computer time Grants 35781029 and 35781035. We wish to acknowledge the strong support of Alan Blumberg, who allowed us to use the ECOM-si coastal ocean circulation model, and Rich Signell, who helped us understand the numerical code. In addition, we want to thank Ken Brink, Dave Chapman, Glenn Flierl, Glen Gawarkiewicz, Hsiao-ming Hsu, Rocky Geyer, Steve Lentz, John Loder, Paola Rizzoli, and Carl Wunsch for their interest in this work and valuable comments and suggestions. Anne-Marie Michael helped prepare the final manuscript, and Jack Cook helped prepare the final figures.

REFERENCES

Blumberg, A. F., 1992: A primer of ECOM3D-si. Tech. Rep., HydroQual, Mahwah, NJ, 66 pp.

——, and G. L. Mellor, 1987: A description of a three-dimensional coastal ocean circulation model. *Three-Dimensional Coastal Models,* Amer. Geophys. Union, 1–16.

Butman, B., R. C. Beardsley, B. Magnell, D. Frye, J. A. Vermersch, R. Schlitz, R. Limeburner, W. R. Wright, and M. A. Noble, 1982: Recent observations of the mean circulation on Georges Bank. *J. Phys. Oceanogr.,* **12,** 569–591.

——; M. Noble, D. C. Chapman, and R. C. Beardsley, 1983: An upper bound for the tidally rectified current at one location on the southern flank of Georges Bank. *J. Phys. Oceanogr.,* **13,** 1452–1460.

——, J. W. Loder, and R. C. Beardsley, 1987: The seasonal mean circulation: observation and theory. *Georges Bank,* R. H. Backus, Ed., The MIT Press, 125–135.

Casulli, V., 1990: Semi-implicit finite-difference methods for the two-dimensional shallow water equations. *J. Comput. Phys.,* **86,** 56–74.

Chapman, D. C., 1985: Numerical treatment of cross-shelf open boundaries in a barotropic coastal model. *J. Phys. Oceanogr.,* **15,** 1060–1075.

Chen, C., 1992: Variability of currents in Great South Channel and over Georges Bank: observation and modeling. Ph.D. thesis, MIT/WHOI Joint Program, Woods Hole, MA, 288 pp.

——, and R. C. Beardsley, 1995: A numerical study of stratified tidal rectification over finite-amplitude banks. Part I: Symmetric Banks. *J. Phys. Oceanogr.,* **25,** 2090–2110.

Flagg, C. N., 1987: Hydrographic structure and variability. *Georges Bank,* R. H. Backus, Ed., The MIT Press, 108–124.

Greenberg, D. A., 1983: Modeling the mean barotropic circulation in the Bay of Fundy and Gulf of Maine. *J. Phys. Oceanogr.,* **13,** 886–904.

LeBlond, P. H., and L. A. Mysak, 1978: *Waves in the Ocean.* Elsevier Scientific, 602 pp.

Limeburner, R., and R. C. Beardsley, 1989: Lagrangian circulation in the Great South Channel and on Georges Bank during summer. *Proc. Third Georges Bank Research Workshop,* Bedford Institute of Oceanography, 29 pp.

Loder, J. W., 1980: Topographic rectification of tidal currents on the sides of Georges Bank. *J. Phys. Oceanogr.,* **10,** 1399–1416.

——, and D. G. Wright, 1985: Tidal rectification and front circulation on the sides of Georges Bank. *J. Mar. Res.,* **43,** 581–604.

——, D. Brickman, and P. W. Horne, 1992: Detailed structure of currents and hydrography on the northern side of Georges Bank. *J. Geophys. Res.,* **97,** 14 331–14 352.

Maas, L. R. M., and J. T. F. Zimmerman, 1989a: Tide-topography interaction in a stratified shelf sea, I: Basic equations for quasi-nonlinear internal tides. *Geophys. Astrophys. Fluid Dyn.,* **45,** 1–35.

——, and ——, 1989b: Tide-topography interaction in a stratified shelf sea, II: Bottom trapped internal tides and baroclinic residual currents. *Geophys. Astrophys. Fluid Dyn.,* **45,** 37–69.

Marsden, R. F., 1986: The internal tide on Georges Bank. *J. Mar. Res.,* **44,** 35–50.

Mellor, G. L., and T. Yamada, 1982: Development of a turbulence closure model for geophysical fluid problem. *Rev. Geophys. Space Phys.,* **20,** 851–875.

Moody, J. A., B. Butman, R. C. Beardsley, W. S. Brown, P. Daifuku, J. D. Irish, D. A. Mayer, H. O. Mofjeld, B. Petrie, S. Ramp, P. Smith, and W. R. Wright, 1984: Atlas of tidal elevation and current observations on the northeast American continental shelf and slope. *U.S. Geol. Surv. Bull.,* **1611,** 122 pp.

Uchupi, E., and J. A. Austin, 1987: Morphology. *Georges Bank.* R. H. Backus, Ed., The MIT Press, 25–29.

Wright, D. G., and J. W. Loder, 1985: A depth-dependent study of the topographic rectification of tidal currents. *Geophys. Astrophys. Fluid Dyn.,* **31,** 169–220.

Zimmerman, J. T. F., 1978: Topographic generation of residual circulation by oscillatory tidal currents. *Geophys. Astrophys. Fluid Dyn.,* **11,** 35–47.

——, 1980: Vorticity transfer by tidal currents over an irregular topography. *J. Mar. Res.,* **38,** 601–630.

——, 1981: Topographical rectification: a comment on spectral representation. *J. Phys. Oceanogr.,* **11,** 1037–1039.